

## Influence of the Narrow {111} Planes on Axial and Planar Ion Channeling

M. Motapothula,<sup>1,2</sup> Z. Y. Dang,<sup>1</sup> T. Venkatesan,<sup>2</sup> M. B. H. Breese,<sup>1,3,\*</sup> M. A. Rana,<sup>4</sup> and A. Osman<sup>5</sup>

<sup>1</sup>Center for Ion Beam Applications, Physics Department, National University of Singapore,  
Lower Kent Ridge Road, Singapore 117542

<sup>2</sup>NUSNNI, National University of Singapore, Singapore 117576

<sup>3</sup>Singapore Synchrotron Light Source (SSLS), National University of Singapore, 5 Research Link, Singapore 117603

<sup>4</sup>Physics Division, Directorate of Science, PINSTECH, P. O. Nilore, Islamabad, Pakistan

<sup>5</sup>National Centre for Physics (NCP), Shahdara Valley Road, Islamabad, Pakistan

(Received 16 January 2012; published 7 May 2012)

We report channeling patterns where clearly resolved effects of the narrow {111} planes are observed in axial and planar alignments for 2 MeV protons passing through a 55 nm [001] silicon membrane. At certain axes, such as  $\langle 213 \rangle$  and  $\langle 314 \rangle$ , the offset in atomic rows forming the narrow {111} planes results in shielding from the large potential at the wide {111} planes, producing a region of shallow, asymmetric potential from which axial channeling patterns have no plane of symmetry. At small tilts from such axes, different behavior is observed from the wide and narrow {111} planes. At planar alignment, distinctive channeling effects due to the narrow planes are observed. As a consequence of the shallow potential well at the narrow planes, incident protons suffer dechanneled trajectories which are excluded from channeling within the wide planes, resulting in an anomalously large scattered beam at {111} alignment.

DOI: 10.1103/PhysRevLett.108.195502

PACS numbers: 61.85.+p

We recently described the fabrication of perfectly crystalline, 55 nm thick silicon membranes [1] which are ideal for observing ion channeling patterns exhibiting a highly nonequilibrium transverse momentum distribution of the channeled beam during its initial propagation. The reduced multiple scattering through such ultrathin layers allows fine angular structure to be observed [1], previously only predicted in simulations [2–5].

This study takes advantage of the diversity of new channeling phenomena involving fine angular structure which is accessible using ultrathin membranes to reveal the different channeling effects of the narrow and wide {111} planes of silicon. We study whether the asymmetric lattice potential at certain axes including a {111} direction, resulting from the offset in position of the atomic strings at opposing walls of the narrow planes in such diamond cubic structures such as silicon is manifested in channeling patterns from such thin membranes. A better understanding of such channeling and dechanneling behavior is important in bent crystal channeling [6–8] and in the generation of channeling radiation [9–11]. These effects were also studied using Monte Carlo simulations performed using FLUX [12,13], based on the Ziegler-Biersack-Littmark universal potential [14,15], and a binary collision model with an impact parameter dependent algorithm for energy loss. Hereafter, we refer to wide and narrow planes as specifically referring to the {111} direction in silicon.

Figure 1(a) shows a composite set of calculated maps of interatomic axial continuum potentials,  $V(r)$ , at various axes using the universal potential equation which has the same functional form as the Moliere potential [12,13]

within the triangular zone bounded by the [001], [011], and [112] axes, where

$$V(r) = \frac{Z_1 Z_2 e^2}{r} \varphi\left(\frac{r}{a}\right), \quad (1)$$

where

$$\begin{aligned} \varphi\left(\frac{r}{a}\right) &= \sum_i \alpha(i) \exp\left(-\frac{\beta_i r}{a}\right) \\ \alpha(i) &= \{0.1818, 0.5099, 0.2802, 0.02817\}, \\ \beta_i &= \{2, 0.9423, 0.4029, 0.2106\}, \\ a &= 0.8853a_0 / (Z_1^{0.23} + Z_2^{0.23}). \end{aligned} \quad (2)$$

Most atomic potentials exhibit two or three planes of symmetry, reflecting the corresponding symmetry of the atomic strings. However, notable exceptions are found at axes along the {111} direction, such as the  $\langle 213 \rangle$  and  $\langle 314 \rangle$  axes, which have a shallow, asymmetric atomic potential between the narrow planes. This is a result of the diamond cubic lattice of silicon where the two rows of atoms of the narrow planes are at different depths. Tilting along the {111} direction progressively changes their relative offset, producing different asymmetric orientations of the atom rows of the [213] and [314] axes. This asymmetry in the atomic potential is reflected about the horizontal plane in the corresponding axes below the [112] axis, shown for the  $[2\bar{1}3]$  and  $[3\bar{1}4]$  axes. This offset also results in the area between the narrow planes being shielded from the large potential well at the wide planes, producing a shallower, asymmetric potential. Given the different nature of the potentials between the narrow and wide planes, it may

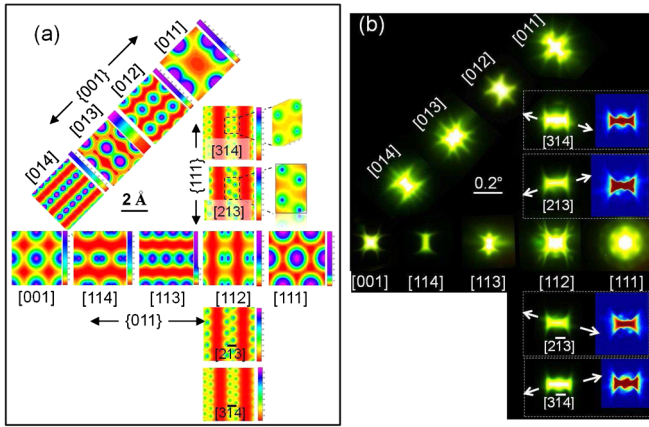


FIG. 1 (color online). (a). Collage of static atomic potentials averaged along the ion direction at different axes away from the [100] axis, at angular locations along (001), (011), (111) planar directions. Also shown are magnified maps of the atomic potential at the [213] and [314] axes. Red (violet) regions represent low (high) potential in the scale bars at each map. (b). Collage of measured axially aligned channeling patterns for 2 MeV protons through a 55 nm [001] silicon membrane at the same axes as in (a). For 2 MeV protons, the axial channeling critical angles of the major axes shown are  $\psi_a[001] = 0.33^\circ$ ,  $\psi_a[011] = 0.41^\circ$ , and  $\psi_a[111] = 0.36^\circ$ . The different orientations of the asymmetric components of the  $\langle 213 \rangle$  and  $\langle 314 \rangle$  axes are shown by arrows. FLUX simulations of the angular distributions are also shown for the  $\langle 213 \rangle$  and  $\langle 314 \rangle$  axes.

indeed be expected that they exhibit distinctly different channeling effects.

Figure 1(b) shows a composite of axial channeling patterns recorded for 2 MeV protons through a 55 nm [001] silicon membrane for the same axes as Fig. 1(a). These patterns were recorded by photographing a highly sensitive aluminum-coated Yttrium aluminium garnet scintillator screen located 50 cm further downstream of the membrane, with a proton beam current of  $\sim 10$  pA, a beam spot size of  $\sim 1 \mu\text{m}$  and convergence angle of  $0.01^\circ$  in a nuclear microprobe, and a camera exposure time of about 0.8 seconds. The planes of symmetry in each pattern correspond to that within the relevant atomic potential map, with none for the  $\langle 314 \rangle$  and  $\langle 213 \rangle$  axes which exhibit a bright, symmetric, horizontal band, with an asymmetric component to either side, differently oriented for the two axes. FLUX simulations confirm that these patterns change with layer thickness but remain asymmetric until the fine angular structure is lost due to multiple scattering in layers thicker than about 100 nm. The asymmetry is reflected about the horizontal plane in the patterns recorded from the  $\langle 2\bar{1}3 \rangle$  and  $\langle 3\bar{1}4 \rangle$  axes. Figure 1(b) also shows FLUX simulations for 500 000 2 MeV protons for the corresponding  $\langle 213 \rangle$  and  $\langle 314 \rangle$  axes of the emergent angular distribution through a 55 nm layer. In all such FLUX simulations, blue (red) regions correspond to low (high) intensity. Under these conditions the  $\langle 213 \rangle$  axes exhibit strong asymmetry in the location of the two bright dots, which further

simulations show originating from those ions incident on the narrow planes.

Figure 2(a) shows experimental channeling patterns recorded for 2 MeV protons transmitted at small tilts to the  $\langle 314 \rangle$  axis, (uppermost three rows) parallel, and (fourth row) perpendicular to the  $\{111\}$  direction. Figures 2(b)–2(d) show simulated patterns of the angular distribution from those beam portions which are incident on the (b) combined  $\{111\}$  planes, and only the (c) wide, (d) narrow planes. On tilting parallel to the  $\{111\}$  direction, the experimental patterns exhibit two components, a bright, horizontal band, which simulations show originating from the wide planes, and a small ringlike “doughnut” [16] structure originating from the narrow planes. Channeling patterns originating from the wide planes do not change with tilt; note that at the  $\langle 314 \rangle$  (and  $\langle 213 \rangle$ ) axes the potential along the wide planes is quite uniform, unlike, e.g., at the  $\langle 111 \rangle$  and  $\langle 112 \rangle$  axes, producing behavior with similar characteristics to that observed in planar channeling on

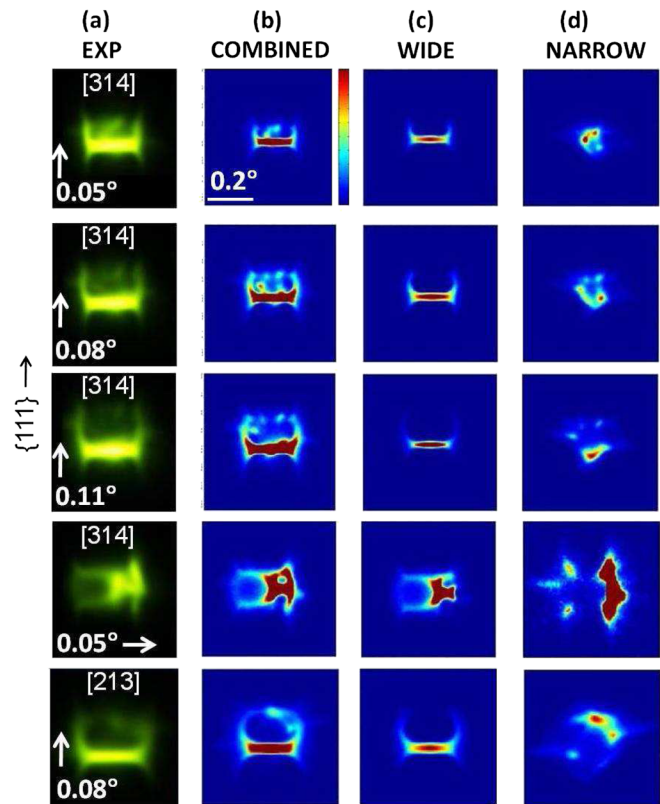


FIG. 2 (color online). (a) Experimental and (b-d) simulated channeling patterns for 2 MeV protons transmitted through a 55 nm [001] silicon membrane close to the  $\langle 314 \rangle$  axis, tilting (top 3 rows) within the vertically-running  $\{111\}$  direction, and (fourth row) across the  $\{111\}$  direction, and (bottom row) for a small tilt away from the  $\langle 213 \rangle$  axis parallel to the  $\{111\}$  direction. The simulated patterns show the angular distribution in the (b) combined planes, (c) wide planes, and (d) narrow planes. The color scales are individually adjusted to best highlight low contrast features.

tilting [17–20]. In contrast, the ringlike patterns originating from the narrow planes increase in diameter with tilt angle, more in keeping with “axiallike” behavior observed at major axes [16]. Figure 2, fourth row, shows that the narrow and wide planes also produce different behavior on tilting perpendicular to the  $\{111\}$  direction. Simulations show that the wide planes produce a circular distribution as typically observed at small tilts away from an axis whereas the narrow planes produce the vertically-running, right-hand line, more in keeping with what may be expected at a planar potential. Thus, not only do the wide and narrow  $\{111\}$  planes produce distinct components in axial channeling patterns, but each may exhibit characteristics of axial or planar channeling, depending on the direction of tilt. Figure 2, bottom row, shows the behavior for a small tilt away from the  $[213]$  axis parallel to the  $\{111\}$  direction, where an even more pronounced asymmetry is observed from the narrow planes, resulting in patterns which are strongly asymmetric about the tilt direction. This is just observed in experimental patterns which are at the limit of our measurement sensitivity.

We now consider whether the effects of the narrow  $\{111\}$  planes can be similarly observed in planar channeling patterns. The planar channeling critical angle,  $\psi$  and planar oscillation wavelength  $\lambda$  are given by [17–19]

$$\psi = \sqrt{\frac{4Z_1Z_2e^2Nd_pCa_{TF}}{pv}} \quad (3)$$

$$\lambda = \sqrt{\frac{\pi Ed_p}{2Z_1Z_2e^2Na_{TF}}}, \quad (4)$$

where  $Z_1$  and  $Z_2$  are the atomic numbers of the incident and lattice nuclei,  $N$  is the atomic density,  $d_p$  in the planar spacing,  $C \cong \sqrt{3}$ ,  $a_{TF}$  is the Thomas-Fermi screening distance and  $p$ ,  $v$  are the ion momentum and velocity. The planar spacing of the wide and narrow  $\{111\}$  silicon planes are 2.4 Å and 0.71 Å, respectively, giving a ratio of 0.54 between the values in wide and narrow planes, of  $\psi$  and  $\lambda$ , with  $\psi_w = 0.15^\circ$ ,  $\psi_n = 0.08^\circ$ , and  $\lambda_w = 240$  nm and  $\lambda_n = 110$  nm, respectively, for low amplitude trajectories for 2 MeV protons. Since only  $\sim 23\%$  of beam is incident on the narrow planes, together with their small critical angle means that their effects are rapidly lost in thick layers at MeV beam energies, so most previous channeling measurements involving the  $\{111\}$  direction have only considered the wide planes as determining the channeling behavior, with the measured critical angle agreeing with this assumption [19,21].

Figure 3(a) shows channeling patterns recorded for 2 MeV protons incident at small tilts to the vertically-running  $\{111\}$  direction of a 55 nm  $[100]$  silicon membrane, at an angular location chosen as free from interference by any intersecting minor axes. Figure 3(b) shows corresponding FLUX simulations of the exit angular distribution for

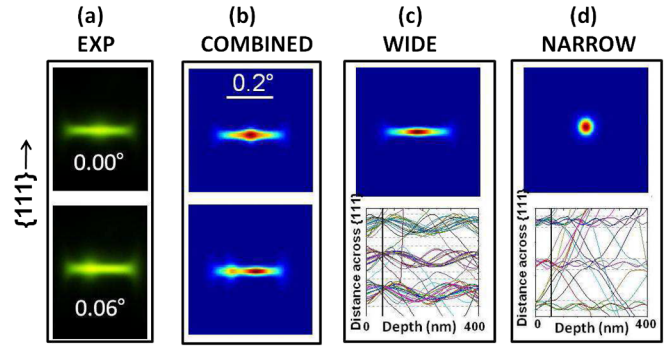


FIG. 3 (color online). (a) Experimental channeling patterns for 2 MeV protons transmitted at tilts of  $0.00^\circ$  and  $0.06^\circ$ . Simulated FLUX channeling patterns for the angular distribution in (b) the combined planes (c,d) in the wide and narrow planes, showing angular distributions at a tilt of  $0.00^\circ$  and channeling trajectories for a tilt of  $0.06^\circ$  for 100 ions to a depth of 400 nm over three adjacent wide or narrow planes. A depth of 55 nm is indicated by a line.

the combined wide and narrow planes for 500 000 2 MeV protons. The experimental and simulated patterns in Figs. 3(a) and 3(b) both exhibit a bump in the planar channeled distribution at small tilts. This feature is not observed in patterns along other major planar directions such as the  $\{001\}$  and  $\{011\}$  which comprise a single plane width. Figures 3(c) and 3(d) show FLUX simulations for beam incident only on the wide and narrow planes, respectively, presenting either exit angular distributions or plots of the channeled trajectories, enabling the origin of the bump to be determined. Along the  $\{111\}$  direction, a layer thickness of 55 nm corresponds to  $\sim \lambda_w/4$  and  $\sim \lambda_n/2$ , so for small beam tilts a large angular spread exits the wide planes but an almost parallel beam exits the narrow planes. The higher electron density within the narrow planes further results in the incident beam being more scattered in the transverse direction compared to the wide planes. These two factors produce the central bump due to the narrow planes, along an otherwise uniform intensity across the wide planes. At a tilt of  $0.06^\circ$ ,  $< \psi_n$ , the bump is displaced in angle away from the  $\{111\}$  direction, because within the narrow planes the beam remains parallel ( $\sim \lambda_n/2$ ), and exits with an angle equal but opposite to its entrance angle.

One observation from the trajectory simulations in Fig. 3(d) is that protons dechanneled from the narrow planes are excluded from channeled trajectories within the wide planes. This is investigated in Figs. 4(a) and 4(c) using FLUX simulations in the form of phase space plots of the beam incident only on the narrow planes, for a tilt of  $0.06^\circ$ . In a phase space representation of planar channeling [22–25] the angular coordinate of the particles is plotted versus its position coordinate relative to the planar channel center. Channeled trajectories occupy a circular or elliptical shape bounded along the position axis by  $x_c$ , this being the closest approach that protons make to the plane walls. The

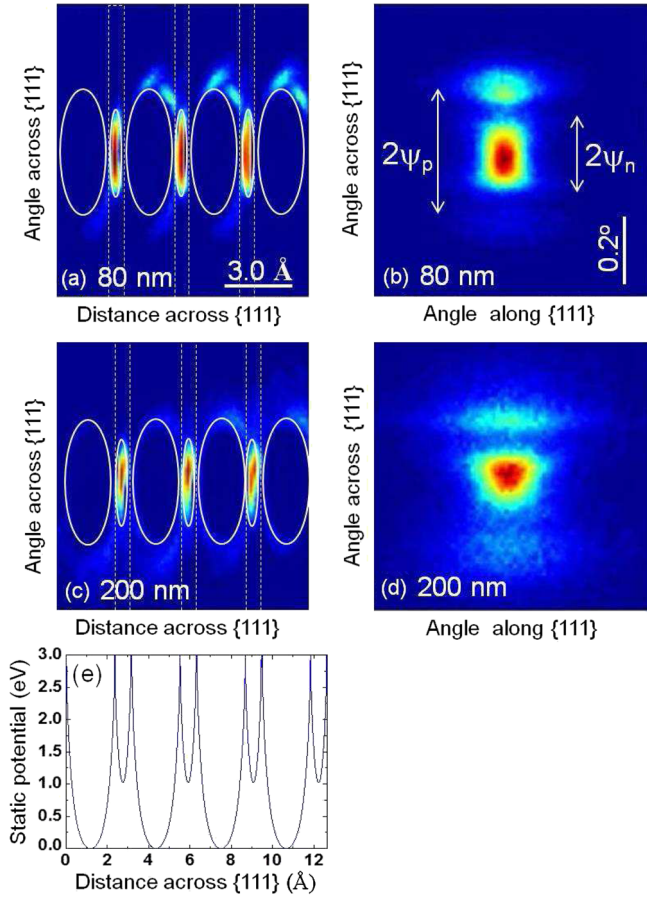


FIG. 4 (color online). (a,c) FLUX simulated phase space ellipses and (b,d) angular distributions at depths of 80 and 200 nm for beam incident on the narrow {111} planes at  $0.06^\circ$  tilt, for 500 000 2 MeV protons. The simulation is over one unit cell, comprising two wide and narrow {111} planes. The extent of the wide and narrow {111} plane ellipses is shown as solid white lines, the lattice plane walls as dashed white lines. The angular distributions are rotated through  $90^\circ$  compared with those in Fig. 3 to give both types of plot the same vertical axis, so in this case the {111} direction is horizontal. (e) Static atomic potential (divided by 8 times) averaged along the ion direction across the {111} planes.

formula  $x_c = d_p/2 - 1.25a_{TF}$  provides good agreement between theory and experiment. Along the angular axis the ellipse is bounded by  $\psi$  and the beam rotates within the ellipse once every  $\lambda$ . Figures 4(b) and 4(d) show the corresponding simulated angular distributions so that the relationship between position and angle is clear.

At a layer thickness of 80 nm, one indeed observes that protons dechanneled from the narrow planes rotate round the outer edge of the phase space ellipse of the wide planes, being excluded from channeled trajectories within them. In a thicker layer, at 200 nm, the coherency of the dechanneled bunches is lost as they merge together, but this thickness conveys the complete exclusion of the dechanneled beam in the wide plane phase space ellipses. The resultant angular distributions, Figs. 4(b) and 4(d), exhibit a bright, central region of the beam portion remaining

channeled within the narrow planes and a narrow, dark band at one or both sides within the angular region ( $\psi_w - \psi_n$ ). The outermost angular components arise from beam oscillating around the outer edge of the wide plane phase space ellipse. The resultant behavior therefore shows beam incident on the narrow {111} planes being rapidly dechanneled and scattered to angles dictated by the wide plane critical angle. Whether this behavior is observed or not depends on the angular distribution of the beam exiting the wide planes.

This behavior may be understood by considering the potential distribution across the {111} planes in Fig. 4(e), comprising a deep well across the wide planes and a shallow well across the narrow planes. Beam incident on the narrow planes requires only a small incident angle,  $\sim \psi_n$  to pass into the deeper potential well of the wide planes where it acquires a transverse angle which is too large to allow capture into a channeled trajectory. Hence, beam incident on the narrow planes exhibits channeling behavior governed by  $\psi_n$  but dechanneling behavior governed by  $\psi_w$ . This same explanation applies to any lattice direction comprising more than one plane width, with the angular scattering of the dechanneled beam fraction determined solely by the widest planes present.

There are two fields where this insight into the dechanneling behavior from the narrow {111} planes is important. One is in extraction of high energy proton beams using bent crystal channeling [6–8], where the silicon {111} rather than the {110} direction is commonly used owing to its larger  $\psi$ . An important consideration is the additional angular spread imparted to the circulating beam in passing one or many times through the bent crystal. Figure 5 shows the simulated angular spread for 2 MeV and 1 GeV proton beams aligned with the {110} and {111} directions. In both cases, rapid dechanneling and consequent large scattering from the narrow {111} planes results in a larger angular spread along the {111} direction. This suggests the {110} direction may be more relevant than previously considered

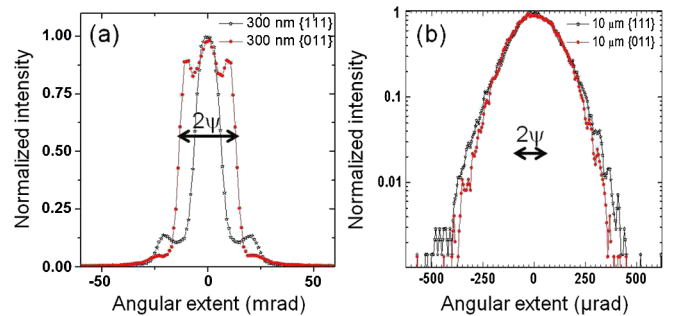


FIG. 5 (color online). FLUX simulated angular distribution across the {110} and {111} directions for (a) 2 MeV protons passing through a 300 nm and (b) a 1 GeV proton beam passing through a  $10 \mu\text{m}$  thick silicon layer. The angular widths,  $2\psi$ , of the {110} and {111} directions is indicated (they are almost identical).

for beam extraction. The other field is the production of channeling radiation, where a high energy charged particle beam is used to induce electromagnetic radiation of keV energies due to the planar channeling action of particles oscillating back and forth between the channel walls [9–11]. Yamamura and Ohtsuki [10] simulated the channeling radiation and its polarization emitted by 56 MeV positrons in silicon and reported a photon spectrum for the {111} direction containing two peaks corresponding to the wide and narrow {111} planes. It is likely that the oscillatory motion of the dechanneled trajectories from the narrow and wide planes in Figs. 3 and 4 will also produce a distinct wavelength of channeling radiation which may be tuned according to the incident planar tilt angle.

This study has revealed the separate ion channeling behavior in narrow and wide {111} planes of silicon. Further studies are in progress on the wealth of fine angular structure which may be observed in such patterns from ultrathin membranes.

---

\*Corresponding author.

†phymbhb@nus.edu.sg

- [1] Z. Y. Dang, M. Motapothula, Y. S. Ow, T. Venkatesan, M. B. H. Breese, M. A. Rana, and A. Osman, *Appl. Phys. Lett.* **99**, 223105 (2011).
- [2] N. Nešković and B. Perović, *Phys. Rev. Lett.* **59**, 308 (1987).
- [3] H. F. Krause, J. H. Barrett, S. Datz, P. F. Dittner, N. L. Jones, J. Gomez del Campo, and C. R. Vane, *Phys. Rev. A* **49**, 283 (1994).
- [4] M. B. H. Breese, D. G. de Kerckhove, P. J. M. Smulders, and D. N. Jamieson, *Nucl. Instrum. Methods Phys. Res., Sect. B* **159**, 248 (1999).
- [5] D. Borka, S. N. Petrović, and N. Nešković, *J. Electron Spectrosc. Relat. Phenom.* **129**, 183 (2003).
- [6] V. M. Biryukov, Yu. A. Chesnokov, and V. I. Kotov, *Crystal Channeling and its Application at High Energy Accelerators* (Springer, Berlin, 1997).
- [7] R. A. Carrigan, Jr. *et al.*, *Phys. Rev. ST Accel. Beams* **5**, 043501 (2002).
- [8] R. P. Fliller, A. Drees, D. Gassner, L. Hammons, G. McIntyre, S. Peggs, D. Trbojevic, V. M. Biryukov, Y. Chesnokov, and V. Terekhov, *Phys. Rev. ST Accel. Beams* **9**, 013501 (2006).
- [9] N. A. Filatova *et al.*, *Phys. Rev. Lett.* **48**, 488 (1982).
- [10] Y. Yamamura and Y. H. Ohtsuki, *Nucl. Instrum. Methods Phys. Res., Sect. B* **2**, 108 (1984).
- [11] C. K. Gary, R. H. Pantell, M. Özcan, M. A. Piestrup, and D. G. Boyers, *J. Appl. Phys.* **70**, 2995 (1991).
- [12] P. J. M. Smulders and D. O. Boerma, *Nucl. Instrum. Methods Phys. Res., Sect. B* **29**, 471 (1987).
- [13] P. J. M. Smulders, D. O. Boerma, and M. Shaanan, *Nucl. Instrum. Methods Phys. Res., Sect. B* **45**, 450 (1990).
- [14] J. P. Biersack and J. F. Ziegler, *Nucl. Instrum. Methods Phys. Res.* **194**, 93 (1982).
- [15] J. F. Ziegler, J. P. Biersack, and U. Littmark, in *The Stopping and Range of Ions in Solids* (Pergamon Press, New York, 1985), p. 41.
- [16] J. S. Rosner, W. M. Gibson, J. A. Golovchenko, A. N. Goland, and H. E. Wegner, *Phys. Rev. B* **18**, 1066 (1978).
- [17] D. Gemmell, *Rev. Mod. Phys.* **46**, 129 (1974).
- [18] L. C. Feldman and B. R. Appleton, *Phys. Rev. B* **8**, 935 (1973).
- [19] *Channeling, Theory, Observation and Applications*, edited by D. V. Morgan (Wiley, London, 1973).
- [20] M. B. H. Breese, P. J. C. King, G. W. Grime, P. J. M. Smulders, L. E. Seiberling, and M. A. Boshart, *Phys. Rev. B* **53**, 8267 (1996).
- [21] L. C. Feldman, J. W. Mayer, and S. T. Picraux, *Materials Analysis by Ion Channeling* (Academic Press, New York, 1982).
- [22] J. A. Ellison, S. T. Picraux, W. R. Allen, and W. K. Chu, *Phys. Rev. B* **37**, 7290 (1988).
- [23] J. A. Ellison, *Nucl. Phys.* **B206**, 205 (1982).
- [24] M. B. H. Breese, E. J. Teo, M. A. Rana, L. Huang, J. A. van Kan, F. Watt, and P. J. C. King, *Phys. Rev. Lett.* **92**, 045503 (2004).
- [25] M. B. H. Breese, M. A. Rana, T. Osipowicz, and E. J. Teo, *Phys. Rev. Lett.* **93**, 105505 (2004).